THE ROYAL SOCIETY

Optical characteristics of synchrotron sources and their influence in the simulation of X-ray topographs

By Y. Epelboin[1], V. Mocella[2] and A. Soyer[1]

[1]*LMCP, UMR 7590 CNRS, Universités P. M. Curie et Paris VII, Case 115, 75252 Paris Cedex 05, France*

[2]*ESRF, Experimental Division, BP 220, 38043, Grenoble Cedex, France*

The optical characteristics of third-generation synchrotron sources and their influence on the simulation of X-ray topographs for various experimental settings, both for the Laue and Bragg case, are discussed. A new generation of simulation programs that allow easy modification of the model of deformation is described.

Keywords: X-ray diffraction; topography; dynamical theory; imaging; simulation

1. Introduction

X-ray topography has been based, in the past, on Lang's (1959) settings: section topography, which allows analysis of a section in the crystal, and traverse or projection topography, where a large volume can be imaged but less quantitative information about the defects is obtained. This latter method is the most widely used in the laboratory, as well as white-beam topography, which is its equivalent at synchrotron stations.

In a section topography, the incident beam is collimated by a very thin slit located in front of the crystal. In each plane of incidence, the width of the beam is very narrow, of the order of 10 μm. The theoretical interpretation of the experiment was made by Kato (1963) on the assumption that the incident beam can been described as a spherical wave located on the entrance surface of the crystal. Thus, the boundary condition, along the surface, reduces to one single point source (figure 1*a*). This simplification has been very successful to explain most features in the formation of the image of the defects (Authier 1967). However, it could not explain some fine features, such as the focalization of the fringes in the image of a stacking fault (Kato 1963; Authier & Sauvage 1966), which was sharper than it appears in real experiments. The common interpretation was that the entrance slit is never as sharp as considered in the theory. This became more evident when the image of a dislocation was first computed by Balibar & Authier (1967). Although the computed white dynamical image, as well as the intermediary image of the defect, was in agreement with the experimental one, it was obviously wrong for the direct image. According to Kato's (1963) theory, a finite entrance slit can be described as a distribution of incoherent sources located along the entrance surface of the crystal (figure 1*b*). The same principle is applied for the understanding of the contrast of a defect in a traverse topography. The distribution of incoherent point sources, along the entrance

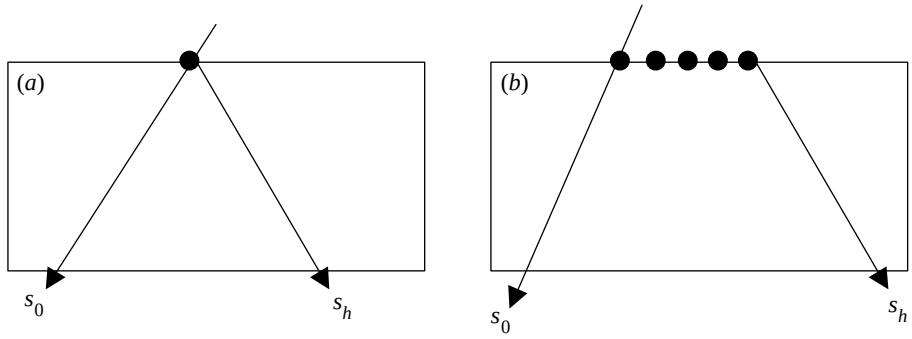

Figure 1. Boundary condition along the entrance surface in Kato's theory: (*a*) a single point source for the section topography; (*b*) a distribution of point sources (incoherent for a traverse topography and a section topography with a finite entrance slit and coherent sources in all other cases).

surface of the crystal, corresponds to the illuminated area in the traverse topography. Difficulties arise when trying to simulate the image because it means that an image is computed adding the contributions of all these sources, and this means lengthy calculations to compute an image (Epelboin & Soyer 1985). This difficulty may be partly lifted applying the reverse principle of optics (Carvalho & Epelboin 1993*a*).

The basic assumption, in Kato's theory, is that the lateral coherence of the incident beam, along the entrance surface, is smaller than the resolution in the film and can be neglected. Thus, each point along the entrance surface can be considered to be incoherent. Kato's approximation is valid if the coherence of the source is less than *ca.* 1μm. As will be explained later, this assumption is valid for laboratory settings because the source-to-crystal distance is small, of the order of 0.5 m, but may become false in the case of a synchrotron, where the distance is much larger. This is especially true for third-generation machines such as ESRF, where this distance is of the order of 150 m.

In the present paper we will study the validity of this model for synchrotron experiments and discuss what it implies for the simulation of the images for the most common settings. In the last part we will briefly describe a new generation of programs that have been designed to easily simulate the images for synchrotron experiments.

2. Limitations to the concept of a distribution of point sources

Let us consider a crystal at Bragg incidence θ located at a distance L_0 from a synchrotron source S (figure 2). The amplitude of the wave at point P, along the exit surface, is made of the contribution of all waves incident along the entrance surface between M and N. We will now study under which condition Kato's assumption is valid, i.e. can we consider a distribution of sources between M and N as a collection of incoherent sources?

One must first underline that this theory has been developed considering the source as a monochromatic point source located on the entrance surface. This assumption is valid if the phase oscillates very rapidly, so that, using the stationary phase method, it is possible to show that the contribution of the source is limited to one single point source. Authier & Simon (1968) have shown that this is valid in the case of

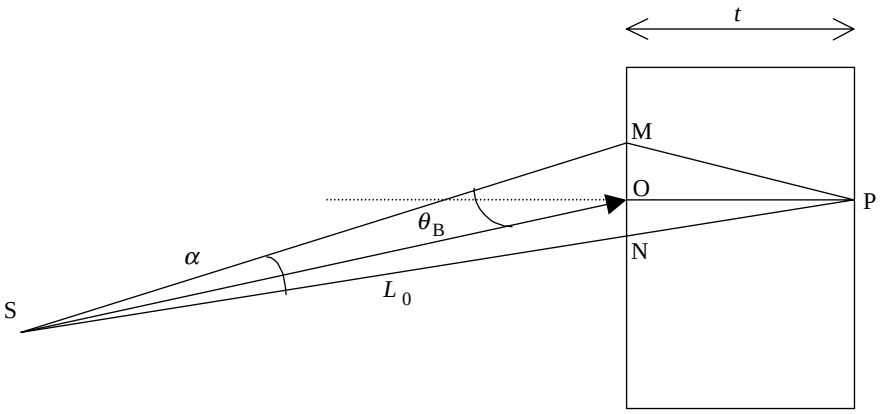

Figure 2. Influence domain of the source S located at distance L_0 from the crystal. It corresponds to the angle of aperture α corresponding to the length MN along the entrance surface.

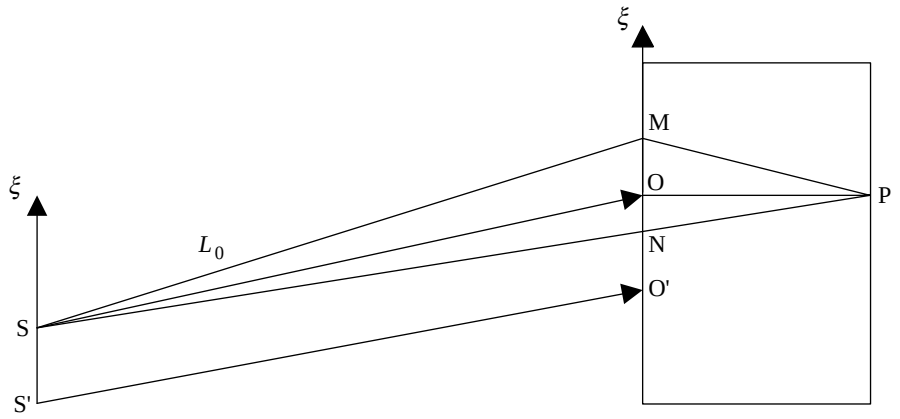

Figure 3. The source S is located at distance L_0 from the crystal. The exact Bragg incidence corresponds to point O. Another point of the source S′ is at exact Bragg incidence at point O′ for the same wavelength.

a section topograph when the source-to-crystal distance is small, as in laboratory settings. If one puts a slit in front of the crystal, the diffraction from the slit must be taken into consideration, even if the result is rather in agreement with Kato's assumption (Aristov *et al*. 1982). At the synchrotron station at ESRF, the situation is completely different since the source-to-crystal distance is of the order of 145 m and the source size is of the order of a few tens of micrometres. The incoming beam may present coherence properties that do not exist in the laboratory. Synchrotron sources also possess another important property: the wavelength spectrum is very wide and can be considered to be white. The polychromaticity can, thus, play an important role and influence the global coherence properties of the incident beam.

Let us first consider a monochromatic point source located at distance L_0 from the crystal. The width $\Delta\theta$ of the rocking curve at half maximum (FWHM) represents the angular acceptance of the crystal. The condition to consider the incident wave as a plane wave, i.e. to neglect the sphericity of the incident wave, is (Born & Wolf 1975) $L_0\Delta\theta^2 \ll \frac{1}{4}\lambda_0$, where λ_0 is the wavelength of the radiation. This condition is

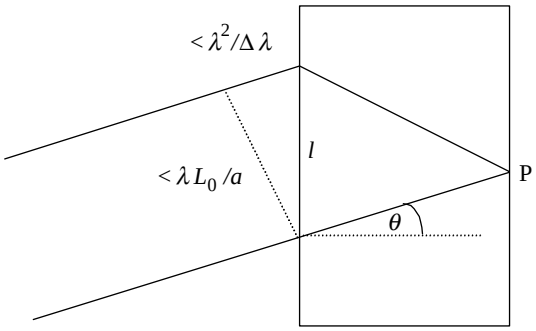

Figure 4. Coherence length $\lambda^2/\Delta\lambda$ and coherence width $\lambda L_0/a$ of the incident wave as a function of the width l of the area, along the surface, contributing to the intensity at point P along the exit surface.

not always fulfilled at modern synchrotron stations such as ESRF. Let us consider a crystal of thickness t and a point P along the exit surface (figure 2). All the contributions come from the part of the incident wave, limited to the base of an inverse Borrmann fan MN $= l$, along the entrance surface. This corresponds to an angular aperture of the source $\alpha = l\cos\theta_{\mathrm{B}}/L_0$, where θ_{B} is the Bragg angle and $l = 2t\tan\theta_{\mathrm{B}}$; t is the thickness of the crystal. If $\alpha < \Delta\theta$, the incident wave may be considered to be a plane wave, which means

$$(2t\sin\theta_{\mathrm{B}})^2/L_0 \ll \tfrac{1}{4}\lambda_0.$$

If the crystal is thin enough, the incident wave may be considered to be 'locally plane'. Typical values for ESRF are a thickness of 700 μm for the 111 reflection for silicon at kiloelectronvolts (Mocella *et al*. 1999*a*). In real experiments the size of the source is finite. The source is made of elementary incoherent sources of size dξ. The calculation of the intensity at point P, along the exit surface, implies a convolution of the intensity profile of the source with the intensity obtained from a single point source. Mocella *et al*. (1999*b*) have shown that this induces a slight complication in the boundary condition, namely for the phase with the introduction of a quadratic term

$$\exp\left(\frac{\mathrm{i}\pi\cos^2\theta}{\lambda_0 L_0}\xi^2\right),$$

where θ is the Bragg angle and ξ is the coordinate along the entrance surface (figure 3). If the source-to-crystal distance is not too small (more than a few metres), this quadratic term does not oscillate too rapidly and can be taken into account in a simulation program. For typical laboratory settings this is impossible. The sampling of the sources, along the surface of the crystal, would be so dense that difficulties would arise in the numerical calculation: not only would it dramatically increase the computation time, but also rounding errors would make it difficult to compute the intensity accurately. Thus, one is limited to the simulation of a single point source located along the surface, as in Kato's assumption.

We must now take into consideration the polychromaticity of the beam. It decreases the coherence of the wave. The relevant bandwidth is of the order of the Darwin width, as expressed as a function of the wavelength. An incident plane wave can be considered to be coherent (Carvalho & Epelboin 1990) if both the coherence

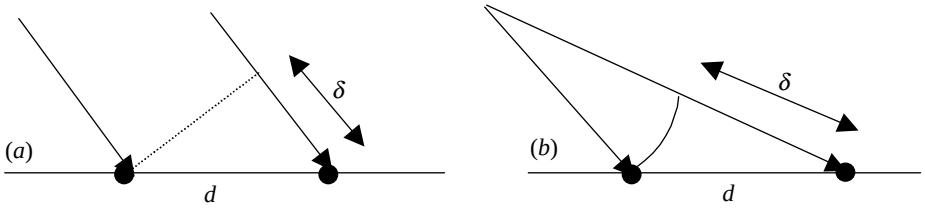

Figure 5. Variation of the phase shift $\Delta\Phi = 2\pi\delta/\lambda$ as a function of the distance d between two point sources in the case of an incident plane wave and an incident spherical wave. $\Delta\Phi$ is constant for a uniform distribution of sources in the case of an incident plane wave, varies more and more rapidly in the case of an incident spherical wave.

length, $\lambda_0^2/\Delta\lambda$, and the coherence width, $\lambda_0 L_0/a$, are smaller than the influence width l (figure 4). a is the source size. This means that both conditions,

$$t < \frac{\lambda_0^2}{\Delta\lambda}\frac{\cos\theta}{\sin^2\theta} \quad \text{and} \quad \frac{\lambda L_0}{a} < 2t\tan\theta$$

must be fulfilled. This is not the case at ESRF, which explains why the polychromaticity destroys the coherence and why, from the theoretical point of view, an incident white beam can be considered to be a distribution of incoherent sources along the surface of the crystal. This explains the similarity between laboratory traverse topographs and white-beam synchrotron topographs (Tanner *et al*. 1977), and why they may be simulated using the same programs (Carvalho & Epelboin 1993*b*).

3. Simulation of X-ray topographs

We can now summarize the different possibilities of simulating X-ray topographs as follows.

1. Section topography: one incoherent point source along the surface (figure 1*a*)
2. Plane-wave topography: a distribution of monochromatic coherent sources (figure 1*b*).
3. Extended spherical wave: a distribution of monochromatic coherent sources (figure 1*b*).
4. White-beam synchrotron and traverse topography: a distribution of incoherent sources along the surface (figure 1*b*).

One must sum the intensity contributions of all the sources.

Cases 2 and 3 differ by the relation between the phases of the point sources located on the entrance surface. In the case of a plane wave, the phase difference $\Delta\Phi$ is constant (assuming a uniform distribution of the sources), but varies more and more rapidly when the departure from exact Bragg incidence increases in the case of an extended spherical wave (figure 5). It means that it might be difficult to correctly sample the phase, for a large aperture of the incident beam, when the distance between the source and the crystal is small, as in a laboratory setting (Epelboin 1977). It is feasible in the case of ESRF since the radius of the spherical wave is large. However, useful settings correspond either to the case of an incident monochromatic

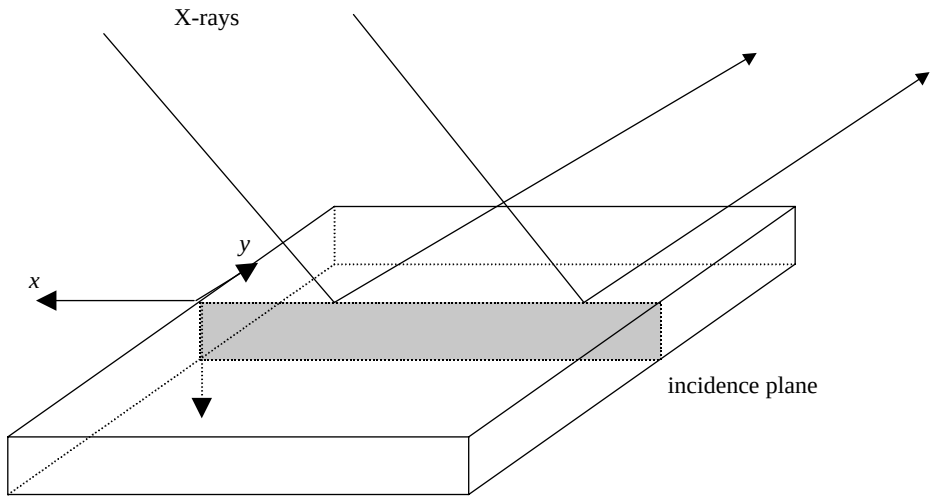

Figure 6. Principle of the computation of a line in an image using the Bragg case as example. Only the data for the deformation in one plane of incidence are required to compute this line. These data are computed separately in a previous program and stored on disk.

plane wave (case 2), an incident polychromatic spherical wave (case 4), or seldom, to case 1 when a very thin slit is put in front of the crystal. Case 3 is not of practical interest and, thus, is never considered in simulation.

The topographic suite is a set of simulation programs that has been written to compute the images and rocking-curve profiles for most experimental settings (cases 1, 2 and 4), either for Bragg or Laue geometry and for any kind of defect.

The amplitude Φ of the diffracted field is the solution of a set of partial hyperbolic derivative equations (Carvalho & Epelboin 1993*b*) in which the local deformation $\boldsymbol{u}(\boldsymbol{r})$ appears in the derivative

$$\frac{\partial}{\partial s_h}(\boldsymbol{h}\cdot\boldsymbol{u}(\boldsymbol{r})),$$

where $\boldsymbol{h}$ is the reciprocal lattice vector corresponding to the reflection and s_h is the diffraction direction. The derivatives of the deformation, i.e. the strain components, have been, in previous programs, computed together with the propagation of the waves. This means that it is necessary to modify the simulation program each time one wants to study a new model for the deformation. Taking advantage of the large memory and disk space available on modern computers, this new generation of programs is based on a full separation of the computation of the deformation induced by the defect and of the computation of the Takagi–Taupin equations (Epelboin 1996).

The end-user writes his own program to compute the strain components for each plane of incidence and stores these data on disk. Then, a simulation program reads these data and computes the Takagi–Taupin equations for each line of the image (figure 6). It is not necessary for the user to be familiar with the numerical techniques used to compute the diffraction. It also allows us to rapidly change the model for the deformation without having to write a new simulation program.

The suite is made of the following.

TRANSQ: simulation of white-beam and traverse topographs in the Laue case.

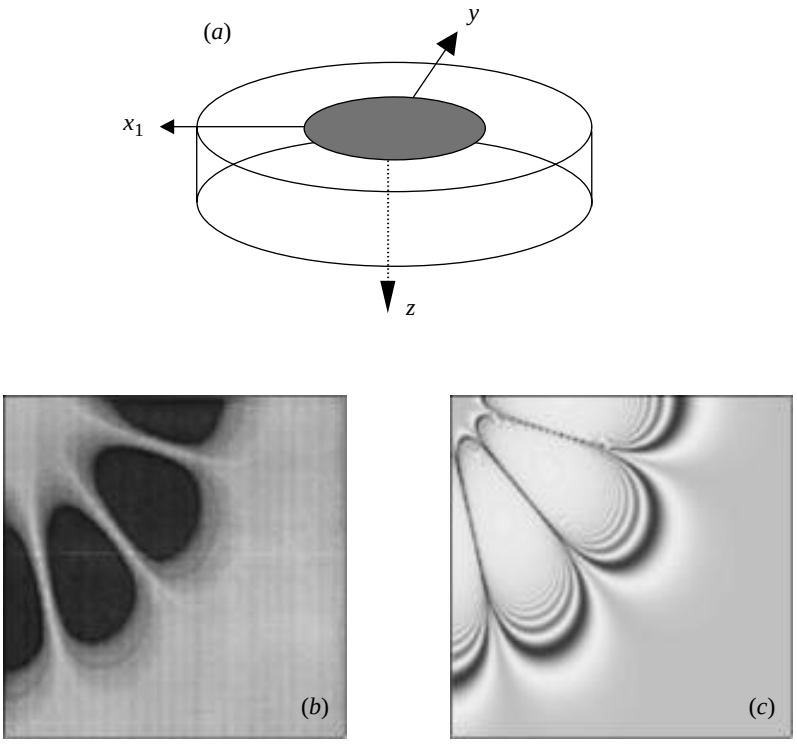

Figure 7. (*a*) Schematic drawing of a piezoelectric quartz device shown with the upper electrode. The entrance surface for the X-rays is on the top. Axes as in figure 6. The diameter is 7 mm. (*b*) Simulation of the white-beam stroboscopic topograph [20] of the device shown in figure 7*a*. λ around 0.76 Å, $\bar{2}1.0$ reflection, size 5×5 mm^2. (*c*) Same as figure 7*b* but plane-wave topograph. $\lambda = 0.76$ Å, $\bar{2}1.0$ reflection, size 5×5 mm^2.

REFPLANE: simulation of plane-wave topographs in the Laue case.

REFRC: computation of rocking-curve profiles in the Laue case.

TOPLANE: computation of plane-wave topographs in the Bragg case.

TOPRC: computation of rocking-curve profiles in the Bragg case.

Since the precision required in the calculation is higher for TRANSQ, it makes use of a more sophisticated algorithm (Carvalho & Epelboin 1993*a*) than the half-step derivative method (Authier *et al*. 1968), which is used in all other programs.

REFRC exists in a special version allowing us to study epilayers. The values of the dielectric χ_h and Fourier $\chi_{\bar{h}}$ components may change, inside the crystal, to simulate a change in the composition of the materials. However, for the sake of simplicity, we assume that the linear absorption μ remains the same throughout the crystal, which means that the zero component χ_0 does not vary dramatically in the epilayer. Since the thickness of an epilayer is usually of the order of 1% of the total thickness or less, this approximation seems acceptable.

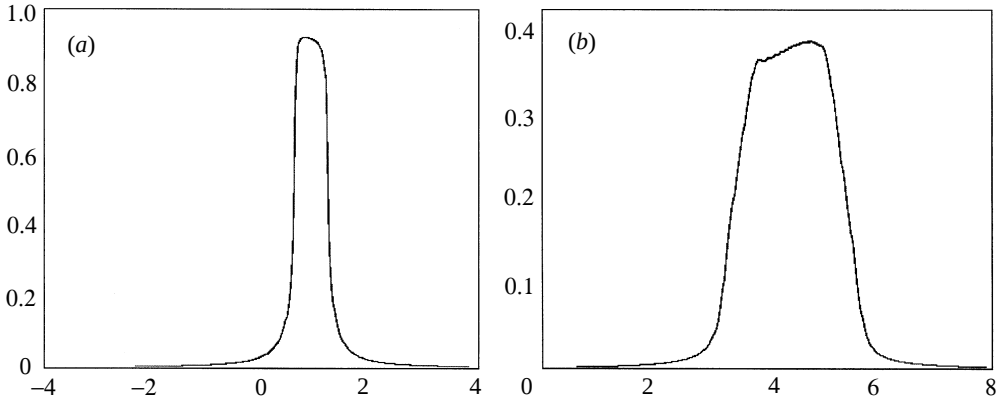

Figure 8. (*a*) Rocking-curve Bragg profile of a perfect silicon crystal, $l = 0.76$ Å, 111 reflection. (*b*) Same profile taking into account the heat load of the crystal at ESRF.

4. Examples of applications

Figure 7 presents the study of a vibrating piezoelectric device. The resonator is made of an AT-cut quartz crystal and it is shaped as a circular plate (figure 7*a*). Figure 7*b* is a stroboscopic white-beam topograph of this crystal. The fringes arise from the shear-mode vibration inside the thickness of the crystal (it has been studied previously by Epelboin *et al*. (1998)). Figure 7*c* corresponds to the same crystal but in a plane-wave experiment. The same strain data have been used in TRANSQ (figure 7*b*) as well as in TOPLANE (figure 7*c*). Figure 7*b* has been computed with an incoherent distribution of sources, figure 7*c* with a coherent one. Details appear in the lobes in the plane-wave topograph, which are not visible in the white-beam topograph since the diffraction is more sensitive to local deformation.

It shows how easy it is to study the same defect for different experimental settings. Once the strain data are calculated, different images may be simulated using the adapted diffraction program.

Figure 8 represents the study of the rocking-curve profile of a silicon plate used as a monochromator at ESRF. Figure 8*a* is the profile of the perfect crystal. Figure 8*b* is the same profile but taking into account the influence of the heat load. The heat dissipation and its influence on the local dilatation of the plate has been computed using a finite-element method (Freund 1998, personal communication). Not only is the FWHM enlarged, but the position of the maximum is shifted. This result is in agreement with the experiment.

The same programs have been used to study a variety of defects such as volumic contrasts in quasi-crystals (Mancini 1998). They can be easily applied to any study, as long as one knows how to compute the strain components.

5. Conclusion

The optical characteristics of the source available at a third-generation synchrotron mean that, under certain considerations such as the large source-to-crystal distance or the thickness of the sample, Kato's approximation of a distribution of point sources along the surface of the crystal may remain valid for most experiments. White-beam topographs may be simulated as an incoherent distribution, summing the intensities

diffracted by all the sources; plane waves or incident spherical waves may be simulated by a distribution of coherent sources introducing a phase shift between the sources. This is why a new suite of programs allowing the simulation of images for most experimental settings has been written. The decoupling of the computation of the deformation from the integration of Takagi–Taupin equations allows easy modelling of a large variety of defects.

References

Aristov, V. V., Kohn, V. G., Polovinkina, V. I. & Snigirev, A. A. 1982 *Physica Status Solidi* **72**, 483–491.

Authier, A. 1967 *Adv. X-ray Analysis* **10**, 9–31.

Authier, A. & Sauvage, M. 1966 *J. Phys.* **27**, 3.

Authier, A. & Simon, D. 1968 *Acta Crystallogr.* A **24**, 517–526.

Authier, A., Malgrange, M. & Tournarie, M. 1968 *Acta Crystallogr.* A **24**, 126–136.

Balibar, F. & Authier, A. 1967 *Physica Status Solidi* **21**, 413–422.

Born, M. & Wolf, E. 1975 *Principles of optics*. Pergamon.

Carvalho, C. A. M. & Epelboin, Y. 1990 *Acta Crystallogr.* A **46**, 449–459.

Carvalho, C. A. M. & Epelboin, Y. 1993*a* *Acta Crystallogr.* A **49**, 460–467.

Carvalho, C. A. M. & Epelboin, Y. 1993*b* *Acta Crystallogr.* A **49**, 467–473.

Epelboin, Y. 1977 *Acta Crystallogr.* A **33**, 756–767.

Epelboin, Y. 1996 *J. Appl. Crystallogr.* **29**, 331–340.

Epelboin, Y. & Soyer, A. 1985 *Acta Crystallogr.* A **41**, 67–72.

Epelboin, Y., Détaint, J. & Capelle, B. 1998 *J. Appl. Crystallogr.* **31**, 574–582.

Kato, N. 1963 *J. Phys. Soc. Japan* **18**, 1785–1791.

Lang, A. R. 1959 *J. Appl. Phys.* **30**, 1748–1755.

Mancini, L. 1998 Thèse de l'Université J. Fourier, Grenoble, France.

Mocella, V., Epelboin, Y., Guigay, J.-P. & Härtwig, J. 1999*a* *Proc. SPIE.* **3448**, 108.

Mocella, V., Guigay, J.-P., Epelboin, Y., Härtwig, J., Baruchel, J. & Mazuelas, A. 1999*b* *J. Phys.* D **32**, A88–A91.

Tanner, B. K., Midgley, D. & Safa, M. 1977 *J. Appl. Crystallogr.* **10**, 281–286.